CONFERENCE PRE-PRINT

RECENT ADVANCES AT THE GLOBUS-M2 TOKAMAK

N.N. BAKHAREV, A.S. ALEXANDROV, S.E. ALEXANDROV, I.M. BALACHENKOV, M.K. BUTS, F.V. CHERNYSHEV, V.V. DYACHENKO, N.V. ERMAKOV, S.V. FILIPPOV, A.N. GOLYAKOV, V.YU. GORYAINOV, E.Z. GUSAKOV, V.K. GUSEV, A.YU. IVANOV, E.M. KHILKEVITCH, N.A. KHROMOV, E.O. KISELEV, A.N. KOVAL, A.N. KONOVALOV, S.V. KRIKUNOV, A.K. KRYZHANOVSKY, G.S. KURSKIEV, A.S. MAREEV, O.S. MEDVEDEV, A.D. MELNIK, V.B. MINAEV, I.V. MIROSHNIKOV, E.E. MUKHIN, A.N. NOVOKHATSKY, M.I. PATROV, YU.V. PETROV, A.YU. POPOV, A.G. RAZDOBARIN, N.V. SAKHAROV, A.E. SHEVELEV, P.B. SHCHEGOLEV, K.D. SHULYATIEV, O.M. SKREKEL, V.V. SOLOKHA, A.YU. TELNOVA, N.V. TEPLOVA, E.E. TKACHENKO, V.A. TOKAREV, S.YU. TOLSTYAKOV, G.A. TROSHIN, E.A. TYUKHMENEVA, V.I. VARFOLOMEEV, N.S. ZHILTSOV
Ioffe Institute
St. Petersburg, Russian Federation
Email: bakharev@mail.ioffe.ru

A.V. BONDAR, E.N. BONDARCHUK, A.A. KAVIN, I.V. KEDROV, A.B. MINEEV, V.N. TANCHUK, V.A. TROFIMOV, A.A. VORONOVA
JSC «NIIEFA»
St. Petersburg, Russian Federation

E.G. KAVEEVA, K.A. KUKUSHKIN, A.M. PONOMARENKO, V.A. ROZHANSKY, I.YU. SENICHENKOV, A.Y. TOKAREV, A.Y. YASHIN
Peter the Great St. Petersburg Polytechnic University
St. Petersburg, Russian Federation

P.A. BAGRYANSKY, S.V. IVANENKO, A.D. KHILCHENKO, A.N. KVASHNIN, E.I. PINZHENIN, I.V. SHIKHOVTSEV, A.L. SOLOMAKHIN
Budker Institute of Nuclear Physics
Novosibirsk, Russian Federation

A.S. DZHURIK, YU.A. KASHCHUK, S.YU. OBUDOVSKY
Project Center ITER
Moscow, Russian Federation

A.E. KONKOV, P.S. KORENEV
V.A. Trapeznikov Institute of Control Sciences of Russian Academy of Sciences
Moscow, Russian Federation

V.A. SOLOVEY
B.P. Konstantinov Petersburg Nuclear Physics Institute, Kurchatov Institute
St. Petersburg, Russian Federation

E.G. ZHILIN
Ioffe Fusion Technology Ltd
St. Petersburg, Russian Federation

Abstract

The manuscript presents an overview of recent research on the Globus-M2 spherical tokamak. Key topics include: the implementation of new diagnostic tools and a plasma control system; results of wall conditioning using a novel technique; studies of plasma confinement and heating, covering the hot-ion mode and ion cyclotron resonance heating; characteristics of the scrape-off layer and divertor plasma; analysis of various instabilities and their impact on confinement; and the design of the next-generation Globus-3 machine.

1. INTRODUCTION

Globus-M2 is a second generation spherical tokamak. It is featuring a compact design, with major radius R=0.36 m and minor radius a=0.24 m. The machine is currently operating at a toroidal magnetic field of up to B_T=0.95 T, and plasma current up to I_p = 450 kA, aiming to reach design parameters: B_T=1 T, I_p = 500 kA. The primary heating system consists of two neutral beam injectors, each capable of delivering up to P_{NBI}=1MW power. The machine serves as an experimental platform for advancing our understanding of hot plasma physics, with particular emphasis on plasma confinement, heating, fast ion behaviour, instability phenomena, and diagnostic innovations.

2. DIAGNOSTICS AND CONROL

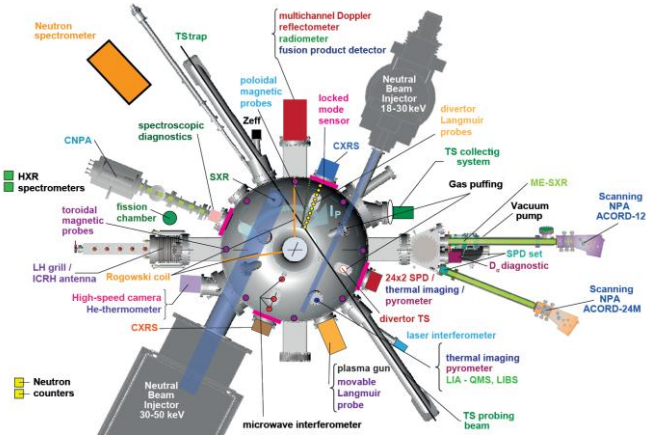

FIG. 1. Globus-M2 experimental layout (top view).

Globus-M2 is equipped with a vast diagnostics complex [1], demonstrated in FIG 1. Over the past two years this complex was supplemented with dispersion interferometer [2], charged fusion product detector [3], two-colour pyrometer [4], locked-mode sensor [5], Silicon Precision Detector array and high-speed cameras [6]. Two new diagnostic tools deserve special mention: Divertor Thomson Scattering (DTS) [7] and the ITER-like U^{235} fission chamber [8]. Both are based on the prototype equipment for the ITER diagnostics.

The installation of an ITER-like U^{235} fission chamber, capable of counting rates up to 2 MHz, has enhanced the temporal resolution of neutron diagnostics on the Globus-M2 tokamak by an order of magnitude. This upgrade enables the observation of fast processes related to energetic ions within the plasma. A key advantage of this system is its capability for autonomous neutron yield monitoring across all operational regimes without the need for a supplementary collimator with an adjustable slit size. Furthermore, a U^{238} fission chamber was tested. It has 1 MeV detection threshold excluding thermal neutrons from the measurement process. These neutrons, scattered by the tokamak structure and the experimental hall, are the primary source of discrepancy between experimental results and simulation data.

DTS diagnostic on the Globus-M2 tokamak provides direct measurements of electron density and temperature in the divertor region. The diagnostic covers the ranges of 1–100 eV in electron temperature T_e and ~10^{17}-10^{20} m^{-3} in electron density n_e. A vertical probing chord crosses the inner divertor leg near the X-point. Scattered radiation is collected from 9 spatial points over ~11 cm (effective spatial resolution ~1 cm), giving access to plasma parameters in the cold, dense divertor plasma, including the inner leg and private flux region. The probing source is a Nd:YAG laser (1064 nm, 2 J, 100 Hz, 3 ns), developed as a prototype within the ITER divertor TS program. The scattered light is analyzed with filter-based polychromators and avalanche photodiodes. The approach to the alignment of the collection optics to the laser beam, proposed for the ITER DTS, was tested in the equatorial Thomson scattering diagnostics [9]. The alignment was monitored in-situ by recording the TS signal from upper and lower halves of alignment fiber bundles. The separation was performed via extra optical path for one of the halves, resulting in 20 ns delay in upper and lower signals. The optics alignment was calculated from the ratio of upper and lower signals and was corrected by stepper motors. Finally, the applicability of the TS hardware in the tokamak control system, which is one of the requirements for the ITER DTS, was demonstrated [10].

Another newly installed diagnostic is the in-situ hydrogen isotope retention diagnostics used on plasma-facing components of the Globus-M2 tokamak [11],[12]. The diagnostics is based on nanosecond laser-induced ablation combined with quadrupole mass-spectrometry (ns-LIA-QMS) to measure deuterium concentrations on divertor tiles. The in-situ measured deuterium surface concentration was varied in the range of $(0.7 – 2.5)\times10^{18}$ D/cm^2, which corresponds to 8-10 at. %. and is comparable with previous results obtained by ex-situ methods.

The optical diagnostic scheme of LIA-QMS is combined with the optical axis for laser-induced breakdown spectroscopy (LIBS) diagnostics, which allows for the elemental analysis of co-deposits in the divertor.

The Globus-M2 tokamak is currently in process of implementation of a new digital plasma equilibrium and shape control system based on a real-time target machine. New FCDI RT [13] code is planned to be used for plasma equilibrium reconstruction in real time based on measurements from 21 magnetic loops and currents in the electromagnetic system windings for application in the control system feedback. Iterative and current filament methods of equilibrium reconstruction in FCDI RT have been tested, a system of isolation amplifiers for transmitting control signals has been developed and implemented, and current control in individual windings has been provided.

3. WALL CONDITIONING

A new wall conditioning technique, termed Inter-Shot Boronization (ISB), has been successfully developed and implemented on the Globus-M2 spherical tokamak, demonstrating advantages over conventional glow discharge boronization (GDB). This technique, utilized during the 2024-2025 experimental campaign, enables continuous in-situ conditioning of plasma-facing components between discharges without dedicated operational breaks. The implementation requires only basic vacuum hardware: a container of solid carborane ($C_2B_{10}H_{12}$) is connected to the vacuum vessel, and its vapours are introduced into the chamber during the approximately ten-minute intervals between plasma pulses. The actual boronization process is inferred to occur during the plasma initiation phase, utilizing the carborane layer pre-deposited on the tokamak wall, with negligible influx during the discharge plateau itself, thus avoiding degradation of the main plasma performance.

The efficiency of ISB is immediately apparent in the decrease of the impurity concentration from shot to shot after ISB start. As illustrated in FIG 2 a), effective charge Z_{eff} exhibits a progressive reduction following the initiation of carborane injection, reaching a plateau after several discharges. When ISB is terminated, Z_{eff} gradually returns to its baseline level. This improvement in impurity control is comprehensively quantified in FIG 2 b), which compares Z_{eff} across experiments with different wall conditioning. The data is obtained at B_T = 0.7-0.8 T, I_p=300 kA, P_{NBI} = 700 kW, 40 keV D neutral beam injection (NBI). ISB allows achievement of Z_{eff} values below 1.1 at $\langle n_e \rangle_V = 2 \cdot 10^{19} m^{-3}$, surpassing the performance of both non-boronized discharges and those following standard GDB. Impurity reduction was further corroborated by decreased loop voltage and diminished emission from intrinsic impurities like carbon, oxygen, and iron, with no evidence of central boron accumulation. Beyond impurity suppression, ISB effectively reduced hydrogen recycling.

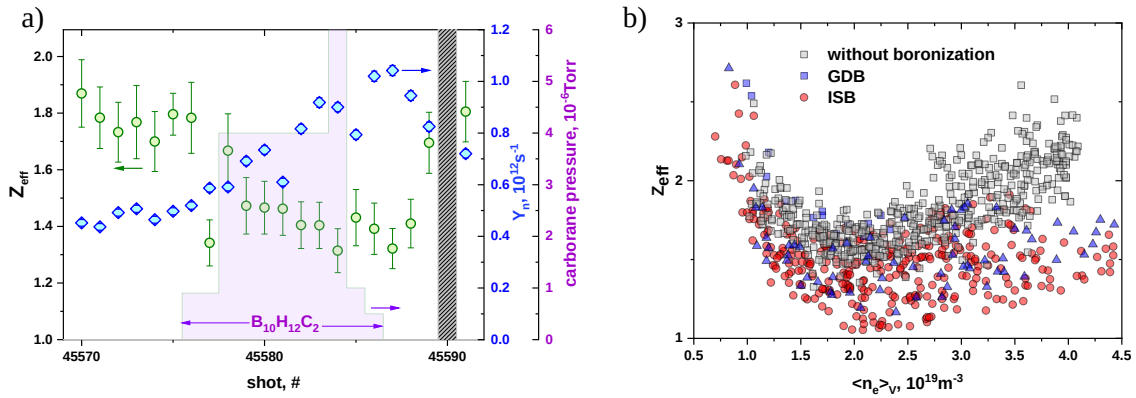

FIG. 2. a) Evolution of the Z_{eff} (green circles) and neutron rate (blue diamonds) during ISB. The violet histogram represents the carborane pressure during ISB. Grey hatched area corresponds to the discharge disruption. Each point is taken at the moment before sawtooth oscillations, when $\langle n_e \rangle_V = 2 \cdot 10^{19} m^{-3}$. b) Dependence of the Z_{eff} on the averaged electron density. Grey squares – discharges without boronization; blue triangles – discharges after GDB; red circles – discharges during ISB.

The most striking result was an unexpected improvement in fast ion confinement. Contrary to predictions that indicated a potential decrease, the neutron yield exhibited a significant increase after ISB initiation, as captured in the discharge-to-discharge evolution shown in FIG 2 a). Neutron rate reached values exceeding twice the pre-

ISB levels, despite deuterium plasma dilution by hydrogen. This doubling of the neutron yield indicates a reduction in fast ion losses, likely attributable to a localized decrease in neutral density, which suppresses charge-exchange fast ion losses. This enhancement directly contributed to a measurable increase in the total stored energy, obtained with diamagnetic loop. However, analysis suggests the thermal energy confinement time remained almost unchanged.

4. HEATING AND CONFINEMENT

4.1. Hot ion mode

A hot-ion mode appears to be a natural operating regime of Globus-M2 during H or D NBI [14],[15] in D plasma at $B_T \geq 0.7$ T. It was successfully achieved even in a presence of sawtooth oscillations. The maximum central ion temperatures (4.7 keV for D NBI and 2.9 keV for H NBI) were obtained at an average density of $\langle n_e \rangle \approx 0.5 \cdot 10^{20}$ m^{-3}. As the density increases, the ion temperature decreases and approaches the electron temperature due to enhanced ion–electron collisional heat exchange (FIG 3 a). Analysis of the experimental data shows that, in the case of D NBI, the thermal energy confinement time τ_E reaches 12–16.5 ms, nearly twice the values obtained with hydrogen injection. Moreover, deuterium injection provides higher ion temperature and toroidal rotation velocity (FIG 3 b). This improvement is attributed to more effective ion thermal insulation: with hydrogen injection the ion thermal conductivity is anomalous (FIG 4 a), whereas with deuterium injection is close to the neoclassical level (FIG 4 b). At the same time, the difference in the average ion mass of the plasma between hydrogen and deuterium injection is only about 12%. In contrast, the central ion temperatures and toroidal rotation velocities differ more strongly. Linear gyrokinetic modeling indicates that at ion temperatures of ~4 keV in the plasma core, the temperature gradient is sufficient to drive ITG turbulence at normalized minor radius r/a=0.7. However, deuterium injection transfers a significant toroidal momentum to the plasma, sufficient to partially or fully suppress this instability via ExB shear. As a result, heat fluxes are reduced to the neoclassical level.

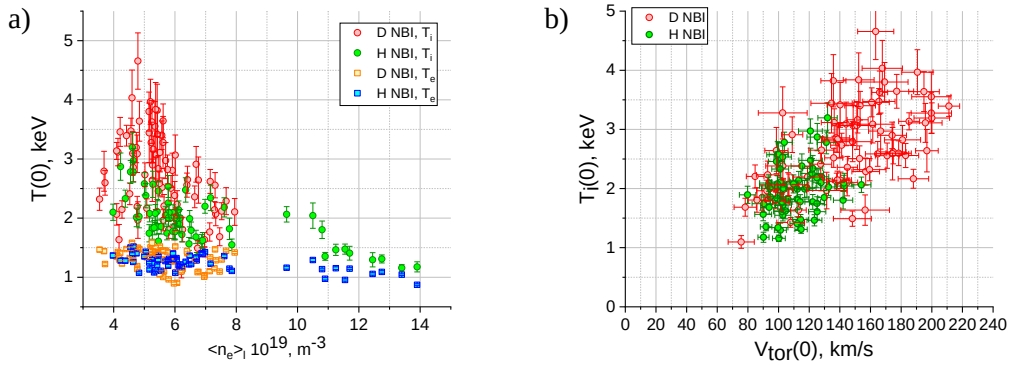

FIG. 3. a) Central ion and electron temperature vs line-averaged electron density. b) Central ion temperature vs toroidal rotation velocity.

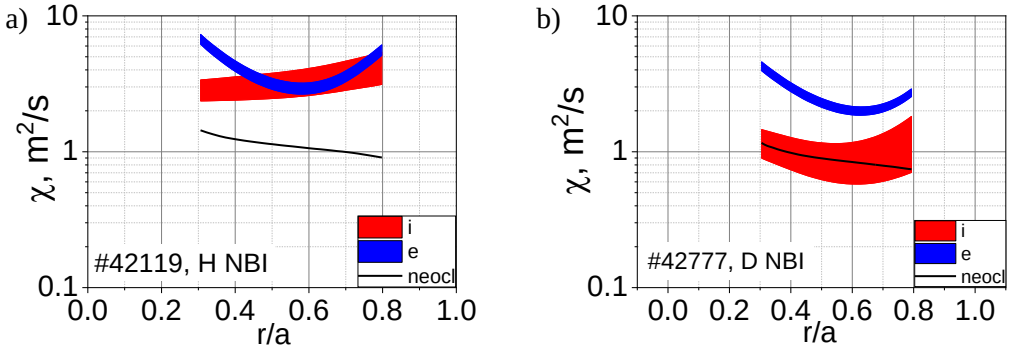

FIG. 4. Thermal conductivities for electrons and ions in D plasma, estimated by ASTRA code for a) H NBI and b) D NBI.

An increase in I_p and B_T leads to an increase in the electron temperature due to improved electron thermal insulation. A comparative analysis of the energy balance showed that with an increase in B_T and I_p by 1.3 times at the same P_{NBI}, the energy confinement time increases by 1.6 times, which is consistent with the predictions of previously obtained scalings for spherical tokamaks. Thermal insulation of ions is much better than that of electrons, and τ_E is determined primarily by the electron component of the plasma. Stability analysis in the gradient zone r/a=0.7 suggests that electromagnetic instabilities like microtearing modes and kinetic ballooning modes are unlikely due to low values of β_e<3%. In contrast, electrostatic electron temperature gradient modes appear unstable and determine the electron heat transport in the considered regimes.

A hot ion mode was also achieved on the ST40 tokamak at higher B_T of 1.7–2 T [16],[17]. FIG. 5 presents a comparison of the H-factor (the ratio of energy confinement time to predictions of IPB98(y,2) scaling) versus B_T and average heat diffusivity versus effective collisionality, combining data from Globus-M2 and ST40. Thermal confinement improves significantly with increasing toroidal magnetic field. However, this trend saturates at an H-factor of ~1.4, indicating a limit to confinement enhancement in spherical tokamaks with further B_T increase. Despite a twofold difference in B_T between ST40 and Globus-M2, the magnitudes of the ion and electron heat diffusivities are remarkably similar (FIG. 5, b). This further supports the hypothesis of scaling saturation and emphasizes that predictive modeling of plasma parameters for future spherical tokamaks using such scalings should be approached with caution.

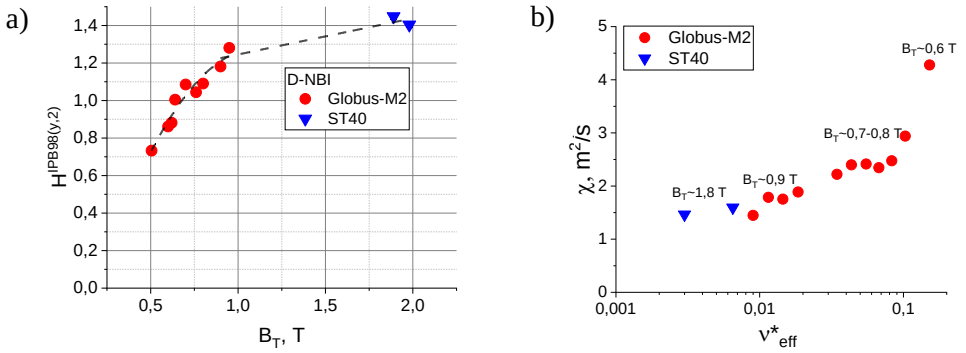

FIG. 5. (a) Dependence of the H-factor on the toroidal magnetic field for Globus-M2 and ST40 data [17]. (b) average heat diffusivity vs collisionality for Globus-M2 and ST40 data [17].

4.2. Ion cyclotron resonance heating

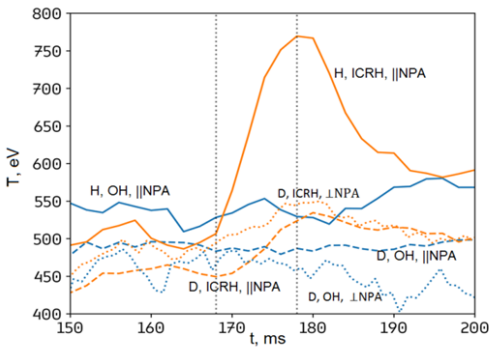

FIG. 6. Effective temperature of hydrogen (solid line) and deuterium (dashed line, dotted line) in the discharges with (#44709, orange) and without (#44707, blue) ICRH, measured with tangential NPA ACORD-24M (||NPA) and perpendicular NPA ACORD-12 (⊥NPA). Vertical lines show time when ICRH is on.

Novel experiments with ion cyclotron resonance heating (ICRH) were conducted in spherical tokamak Globus-M2 with magnetic field larger than B_T=0.7 T. Ion temperature and energy distribution of suprathermal particles were measured using the neutral particle analyzers (NPA). Utilizing a two-ion species scheme (H-D) in Ohmic (OH) plasmas, ICRH at 11.4 MHz generated ions with energies surpassing 20 ion temperatures (22.5 keV), the hydrogen temperature increased by 50% while deuterium temperature growth were at moderate 15%. An example of ion temperature evolution is shown in FIG 6. Application of ICRH in the deuterium discharges with 30 keV NBI demonstrated the increase of the 35 keV ion concentration up to ten times. A three-ion species scheme (H-D-^{3}He) employing ICRH at 5.7 MHz produced a localized 15% electron temperature growth in vicinity of the fundamental helium-3 resonance spatial location.

5. SOL

5.1. High Field Side High Density

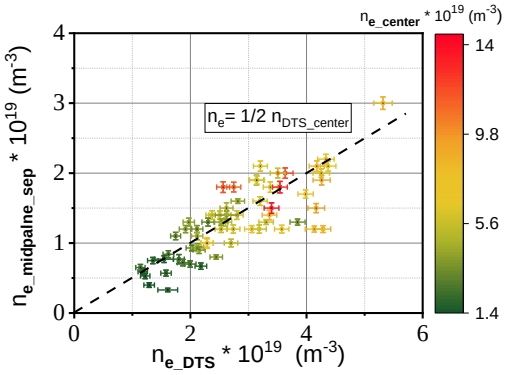

FIG. 7. TS measurements during quasi-stationary phase of 18 discharges: n_e at the plasma center (colored) and on the separatrix (vertical axis) measured by midplane TS as a function of the maximum n_e measured by DTS (horizontal axis).

High Field Side High Density (HFSHD) previously discovered on DIII-D, JET and ASDEX has been discovered in Globus-M2 [18]. It was observed during quasi-stationary phase over a wide range of discharge parameters, with the central n_e ranged from $2{\cdot}10^{19}$ to $1.4{\cdot}10^{20}$ m^{-3}, both with and without 0.7 MW D neutral beam injection (FIG. 7). Measurements of the divertor Thomson scattering show formation of a plasma region with increased n_e, maximized at a distance of ~3 cm from X-point and ~2 cm from the separatrix. The peak n_e in the inner divertor leg measured 1.5 to 3 times higher than n_e on the same magnetic surface at the outer midplane. This experimental data showed agreement with simulation made for the discharge #44644 using the SOLPS-ITER code [19] with a description of deuterium atoms, molecules and carbon atoms, employing the EIRENE code with the Monte Carlo approach (FIG. 8). Identification of HFSHD phenomenon in spherical tokamak is important for enhanced knowledge of the plasma stability mechanisms in tokamaks of this type, and for improving control and optimization of plasma regimes in future machines like a reactor-scale spherical tokamak.

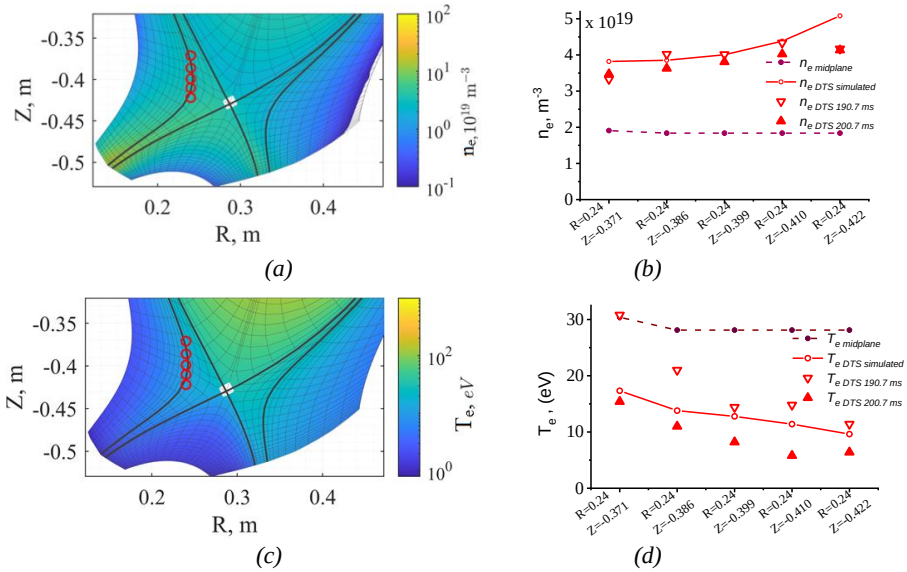

FIG. 8. Comparison of the modelled temperature and density profiles with the profiles measured by DTS. (a) 2D plot of electron density and (b) comparison of density to DTS measurements; (c) 2D plot of electron temperature and (d) comparison of temperature to DTS measurements. DTS measurements points are marked in 2D plots (a) and (c) by red circles.

The increased density region is located between the active and inactive separatrices [20],[21][22], where the cold upper inner target is connected by magnetic tubes with the hot lower inner target. This connection leads to the thermoelectric current, directed towards target in the inner divertor. Poloidal electric field directed towards the target is required for the thermoelectric current to pass through the inner divertor cold plasma layer. Moreover, the electron temperature and pressure are big in this region arranged at the X-point level giving rise to Boltzmann and thermal force contributions to the potential variation. All these effects lead to the elevated electrostatic potential at the X-point level between the separatrices and to the corresponding electric field. In contrast, in the far SOL beyond the inactive separatrix the thermoelectric current, the electron temperature and

density and their variations are low. Therefore, the regions of high electric field and corresponding drifts are all localized between the separatrices. The radial *ExB* drift of ions and electrons in the direction of the strong magnetic field leads to the formation of a region of increased density. The distribution of the electrostatic potential in the divertor region together with the directions of *ExB* and *grad B* ions flows are shown in FIG. 9. It is interesting to note that, in Globus-M2, the *grad B* drift contributes significantly to plasma transport through the separatrix below the X-point. As it is found in the simulation, *grad B* drift flow through the separatrix is approximately twice lower by absolute value than the flux associated with the *ExB* drift for the inner divertor leg, and equals to approximately 30% of *ExB* flux in the outer divertor. In both divertors, this *grad B* flux is directed towards the private flux region, thereby reducing the effect of electric drift in formation of the high-density region. The total drift flux (including the contributions of the *ExB* and *grad B* drifts) through the separatrix of the inner divertor equals to approximately 50% of the ion flux to the inner target between the separatrices, thus significantly changing the particle balance in the inner divertor region.

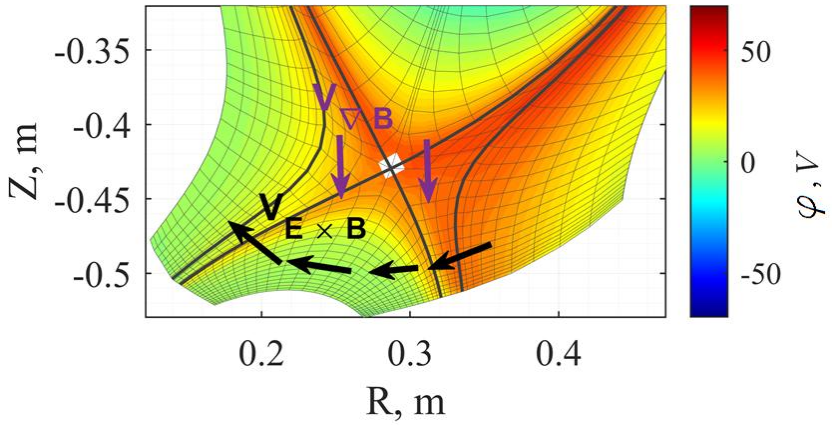

FIG. 9. Map of electrostatic potentials and directions drift flows in divertor region.

5.2. SOL power decay length

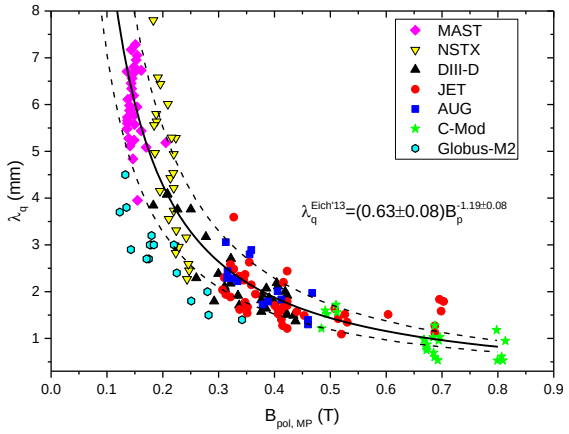

FIG. 10. Poloidal magnetic field at the outer midplane versus power fall-off length.

In the recent experimental campaign the divertor heat flux has been measured using infrared thermography in a series of inter-ELM H-mode discharges. The obtained heat flux profiles were fitted using the Eich formula [23]. It allows the power fall-off length at the midplane (λ_q) to be extracted by accounting for the flux expansion from the midplane to the target. The λ_q was determined for a range of plasma parameters, including toroidal field (B_T=0.5-0.95 T) and plasma current (I_p=155-400 kA), with NBI heating power not exceeding 0.8 MW. The results were compared with multi-machine scaling of the power fall-off length [24]. The dependence on the plasma current (or equivalently the poloidal magnetic field at the outboard midplane) is illustrated in FIG. 10. The current Globus-M2 database indicates a scaling of $\lambda_q \sim I_p^{-1}$, which is consistent with trends observed on other tokamaks.

6. INSTABILITIES

6.1. Alfvén instabilities

Alfvén instability studies were conducted across a wide range of plasma parameters (FIG. 11, a): I_p = 160-450 kA, B_T = 0.4-0.9 T, n_e = 10^{19}-10^{20} m^{-3}, E_{NBI} = 20-50 keV, P_{NBI} = 0.3-1.5 MW. The non-dimensional parameter domain v_{fast}/v_a-$\beta_{fast}/\beta_{total}$ (where v_{fast} is velocity of the injected atoms, v_a is Alfvén velocity, β_{fast} is

volume-averaged fast ion beta, β_{total} is the sum of the fast ion and plasma betas) of the experiments with toroidal Alfven eigenmodes (TAE) and energetic particle modes (EPM) at Globus-M/M2 covers domain of the future ITER DD and DT experiments. Using multi-frequency DBS, it was possible to determine the localization of various Alfvén eigenmodes (AEs) [25]. Chirping toroidal Alfven eigenmodes (TAE) were developed inside the last closed flux surface (LCFS) at radii 0.45-0.58 m, but disappeared in the plasma core and edge. Doppler shifted TAEs [26] were detected in a wider region which coincides with the region of the maximum gradient of the rotation velocity. Apart from that, Alfven cascades were found to develop slightly deeper in the plasma, since they develop within the region of the safety factor minimum in the central plasma. The emergence of these AEs was accompanied by changes in the turbulence level and the average poloidal rotation velocity.

The experimental studies demonstrate that TAE-induced fast ion losses lead to localized heating of the first wall. Using a high-temporal-resolution two-color pyrometer [27] and an infrared camera [28], temperature increases of up to 150°C and local heat fluxes reaching ~20 MW/m^2 were measured during TAE bursts. The heat flux consists of two components (FIG. 11 b): a coherent part, synchronous with magnetic probe signals, attributed to direct orbital losses of fast ions, and an incoherent part, which decays more slowly and is linked to charge-exchange losses near the plasma boundary. The incoherent component has a linear growth with amplitude increase above the threshold while the coherent one is better approximated by two linear segments with different slopes. Numerical modeling suggests that the observed experimental data corresponds to resonant convective transport of ions from the plasma core to the edge, and the observed threshold behavior in heat flux versus TAE amplitude is explained not by diffusive transport but by the spatial distribution of fast ions – at low amplitudes, only edge-localized ions are lost, while higher amplitudes allow core ions to reach the wall.

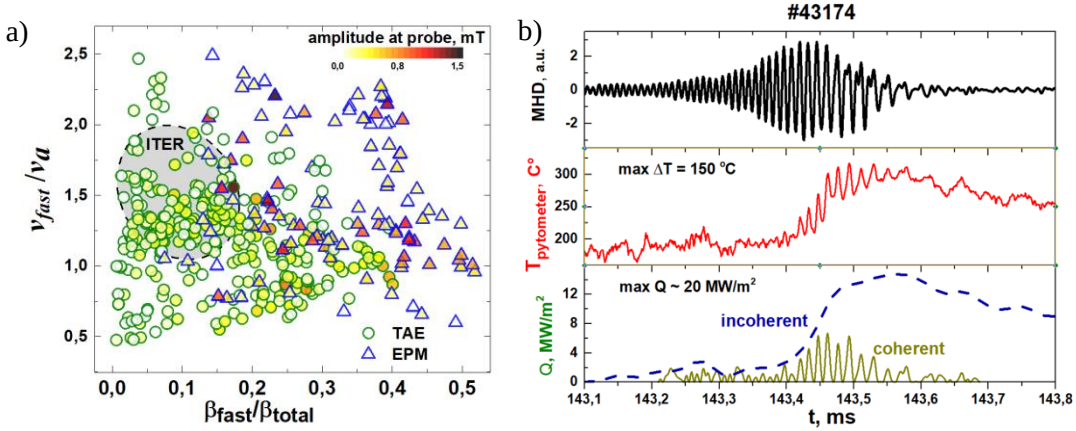

FIG. 11. a) Parameter domain of the Globus-M/M2 experiments with Alfvén eigenmodes b) Experimental measurement of wall heating during TAE development in discharge #43174. From top to bottom: MHD probe signal; wall temperature measured by a pyrometer; coherent (solid line) and incoherent (dashed line) heat flux.

6.2. ELMs

The H-mode on Globus-M2 is regularly accompanied by edge-localized modes (ELMs). A detailed study of high-frequency small ELMs independent from sawtooth oscillations was undertaken in regimes with high pedestal pressure, toroidal magnetic field and plasma current values [29]. It was observed that they can significantly perturb the plasma parameters both outside and inside the LCFS. A systematic change of electron temperature and density profiles was observed: the integrated electron pressure did not change during the ELM cycle but the plasma pressure inside the LCFS decreases and SOL pressure increases. Clear peaks in the floating potential signals measured in the divertor region are synchronized with ELM bursts: the observed electrostatic potential behavior was interpreted based on the analysis of the structure of the SOL and private flux region currents. There is a consistent increase of the turbulence amplitude [30] and perpendicular plasma rotation velocity [31] values during ELMs up to 7 cm inside the LCFS despite no dramatic changes in the pressure profiles in this region. Experimental observations indicate transport of energetic ions and suprathermal electrons to the plasma periphery [32].

6.3. Effect of various triangularity on edge plasma stability

Globus-M2 magnetic equilibrium has an intrinsically high value of triangularity (δ) around 0.4 and elongation around 1.9. It leads to relatively peeling-ballooning stable edge plasma. Despite high parameters in H-mode NBI Globus-M2 discharges, ELMs obtain type-V traits at pedestal pressures higher than p_{ped}= 4 kPa. The recent experiment with varied δ was conducted to investigate the effect of the expansion of plasma volume at the bad curvature region on edge plasma [33]. H-mode discharges with δ around 0.2 and elongation around 1.9 exhibited type-V ELMs onsets with a high frequency around 2 kHz at low pedestal pressure (p_{ped}= 1.2 kPa) [34]. The H-mode discharge with variable δ from 0.18 to 0.21 has shown the corresponding 20% increase in critical pedestal pressure. The simulations using BOUT++ code [35] exhibited the intrinsically unstable peeling–ballooning mode with low toroidal numbers (n ~ 5) in low triangularity discharges. The destabilization of the peeling-ballooning mode at the experimentally observed pressure level is expected according to three-field magnetohydrodynamic simulations.

6.4. Edge harmonic oscillations

ELM-free regimes accompanied by edge harmonic oscillations (EHO) have also been observed on Globus-M2 in weakly shaped discharges (triangularity δ < 0.2) with a large safety factor (q_{95} <= 6) [36]. During such regimes there is an increase of the average electron density, electron temperature and ion temperature, along with a steady decrease of the effective ion charge. An increase of the toroidal rotation velocity as well as the toroidal rotational shear was measured. The perpendicular rotation velocity changes dramatically from -1 km/s up to 3 km/s. The pedestal conditions during this phase of the discharge were close to the peeling-ballooning stability limit in the linear 3-field MHD simulations that used the BOUT++ code. The most unstable mode had low toroidal numbers (n=5). EHO-like oscillations were detected in the form of coherent fluctuations on various diagnostics: a clear peak at the 8 kHz frequency can be observed in the spectra of the D_α signal, fluctuations of magnetic probe (MP) signals amplitude, average electron density, Langmuir probe (LP) floating potential, perpendicular rotation velocity and backscattered power as shown in FIG. 12. The oscillations were primarily detected on edge diagnostics, such as Langmuir probes, and DBS confirmed that the mode developed at the plasma edge at radii 0.56-0.61 m.

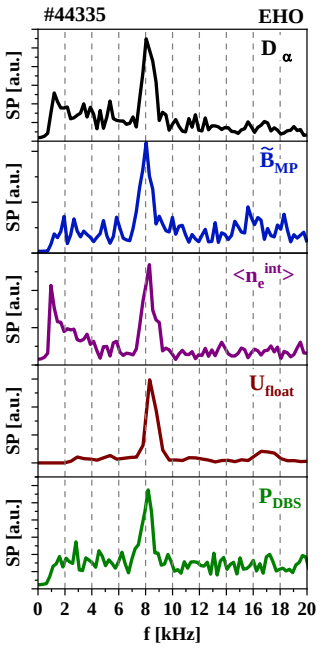

FIG. 12. Spectra of diagnostics signals (from top to bottom) D_α signal, fluctuations of MP signals amplitude, average electron density measured using interferometry, LP floating potential and DBS backscattered power at R = 0.59 m exhibit peaks at 8 kHz

6.5. Locked MHD modes

The impact of error field-induced locked MHD modes on plasma confinement and heating efficiency during NBI was investigated [5]. The onset of these modes is linked to a severe degradation of global plasma parameters: we observed a rapid drop in electron density, soft X-ray emission, plasma energy content and the central ion temperature – which was reduced by a factor of two in affected discharges. The locked mode drives not only a loss of thermal confinement but also fast ion transport or losses, which was evidenced by a drop in neutron flux. To address locked modes, a set of four external correcting coils, capable of generating a tailored horizontal magnetic field to compensate for the dominant n=1 error field component, was installed at the tokamak. In addition, a novel magnetic sensor system with active compensation for toroidal and vertical fields was developed. It allows detecting locked modes, which develop without the preceding rotating MHD island and are absent in the signal of the regular magnetic probe. While implementation of the error field correction system resulted in a substantial decrease of the locked mode occurrence, their appearance remains stochastic. The reasons for their development in some discharges and not in others with similar parameters are not fully understood.

6.6. High frequency oscillations

In Globus-M2 other magnetohydrodynamic instabilities interacting with suprathermal particles were also observed. During experiments with NBI, in addition to the previously discussed Alfvén eigenmodes, a distinct suprathermal ion-driven instability was identified. This instability, known as Ion Cyclotron Emission (ICE), occurs at frequencies corresponding to Doppler-shifted ion-cyclotron harmonics. The source of ICE is localized within the plasma bulk near the magnetic axis [37]. Furthermore, instabilities driven by accelerated electrons were detected in two frequency regimes during Ohmic discharges at low plasma density and lower hybrid current drive (LHCD) experiments. In the sub-ion-cyclotron frequency range (approximately 1-2 MHz) bursts of Fast Magnetosonic Waves were observed [38]. These emissions manifest as chirped oscillations with longitudinal polarization, whose frequency follows Alfvén scaling and shows correlation with n = 1 MHD sawtooth disruptions. At higher frequencies, typically tens of MHz but still below the lower hybrid resonance, so-called magnetosonic whistlers were recorded [38]. These waves are excited by electron beam instability. Notably, magnetosonic whistlers in Globus-M2 were also observed during the discharge quenching phase under conditions of extremely low plasma density, when the plasma current was sustained solely by a runaway electron beam.

7. GLOBUS-3

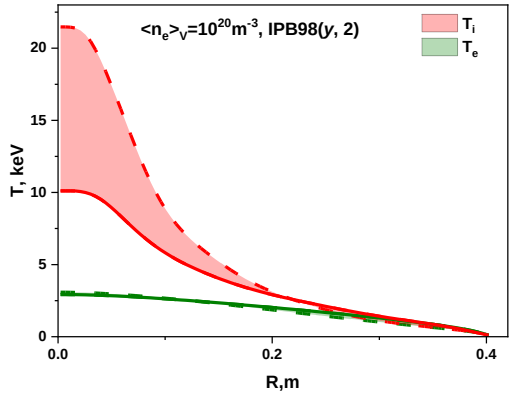

FIG. 13. Temperature profiles in Globus-3. Uncertainty is associated with the unknown peaking factor of the density profile.

Globus-3 represents the next step in the research program on plasma confinement in low-aspect-ratio tokamaks at the Ioffe Institute. Building upon the experience gained with its predecessors, Globus-M and Globus-M2, the key distinguishing features of the new device are a significant increase in both the toroidal magnetic field (1.5 T, with a potential upgrade to 1.8-2.0 T) and the major radius (R_0 = 0.775 m), along with a longer plasma discharge duration exceeding the characteristic times for the formation of stationary plasma parameter profiles. The design features a warm, pulsed electromagnetic system and a vacuum vessel with increased clearance on the low-field side to accommodate antennas for auxiliary heating and current drive systems, including NBI, ICRH, LHCD, and the newly planned Electron Cyclotron Resonance Heating. Simulations for the baseline scenario (B_T = 1.5 T, I_p = 0.8 MA) predict ion temperatures of several keV, while an advanced high-field scenario (B_T = 1.8 T, I_p = 2.0 MA) could achieve ion temperatures of 20 keV even in the case of conservative estimations, based on IPB98(y,2) scaling (FIG. 13), potentially reaching a fusion-relevant temperatures and allowing for studies of MeV-range alpha-particle behaviour from the p + ^{11}B reaction.

ACKNOWLEDGEMENTS

The work was performed on the Unique Scientific Facility "Spherical tokamak Globus-M". Preparation of the routine tokamak diagnostics (section 2) was performed in accordance with the state assignment № 0034-2021-0001. Wall conditioning studies (section 3) was performed in accordance with the state assignment № 0040-2019-0023. Fast ion study (subsection 6.1, 6.6) was supported by RSF research project № 21-72-20007-P. Energy confinement studies (subsection 4.1) were supported by RSF research project № 24-12-00162. Work on the study of divertor plasma (subsection 5.2) was supported by the Russian Science Foundation (23-79-00033). ELM and EHO studies (subsection 6.2, 6.3) were supported by RSF research project № 23-72-00024. Globus-3 development was supported by RSF research project № 21-79-20133-P.

REFERENCES

[1]. PETROV, Yu. V., BAGRYANSKY, P. A., BALACHENKOV, I. M., et al. Diagnostic Complex of the Globus-M2 Spherical Tokamak, Plasma Phys. Rep. **49** 12 (2023) 1459-1479

[2]. IVANENKO, S.V., SOLOMAKHIN A.L., ZUBAREV P.V., et al. Dispersion interferometry diagnostic at Globus-M2, Fusion Engineering and Design. **202** (2024) 114409.

[3]. BAKHAREV, N. N., SKREKEL, O. M., ALEKSANDROV, A. S., et al. The first results of a charged fusion product diagnostics at the Globus-M2 spherical tokamak, Tech. Phys. Lett. **50** 10 (2024) 24-27.
[4]. VORONIN, A. V., GORYAINOV, V. Y., KAPRALOV, A. A., et al. Investigation of the surface temperature in contact with plasma by two-color pyrometry, Technical Physics. **68** 12 (2023) 799-805
[5]. PETROV, Y. V., BALACHENKOV, I. M., BAKHAREV, N. N., et al. Effect of locked MHD modes on the efficiency of plasma heating by the neutral beam injection method at the Globus-M2 spherical tokamak, Plasma Physics Reports. **50** 7 (2024) 773-780.
[6]. TIMOKHIN, V., NOVOKHATSKY A., KOROBKO D. et al. Investigation of filament dynamics using high-speed video shooting in the globus-m2 tokamak, this conference.
[7]. ERMAKOV, N. V., ZHILTSOV, N. S., KURSKIEV, G. S., et al. Divertor Thomson Scattering on Globus-M2, Plasma Physics Reports. **49** 12 (2023) 1480-1489
[8]. KORMILITSYN T.M. et al. "Features of fusion power measurements in the next generation magnetic plasma confinement experiments" 30th IAEA Fusion Energy Conference (Chengdu, People's Republic of China, 2025).
[9]. ZHILTSOV, N. S., KURSKIEV, G. S., TOLSTYAKOV, S. Y., et.al., Thomson scattering diagnostics at the Globus-M2 tokamak, Fusion Engineering and Design. **211** (2025) 114753.
[10]. ZHILTSOV, N. S., KURSKIEV, G. S., SOLOVEY, V. A., et al. Using Thomson scattering diagnostics to control plasma density at Globus-M2 tokamak, Tech. Phys. Lett., **49** 8 (2023) 350-354.
[11]. RAZDOBARIN, A.G., MEDVEDEV, O.S., BUKREEV, I.M. ET al. Laser Diagnostics of Content of Hydrogen Isotopes in the Globus-M2 Tokamak Wall, Plasma Phys. Rep. **50** 6 (2024) 667–677.
[12]. O.S. MEDVEDEV, A.G. RAZDOBARIN, E.V. SHUBINA et al. LIA-QMS method for the quantity analysis of the hydrogen isotopes retention in first-wall components of Globus-M2 tokamak, Nuclear Materials and Energy. **41** (2024) 101829.
[13]. KORENEV, P. S., KONKOV, A. E., MITRISHKIN, Y. V., et al. Improved FCDI algorithm for tokamak plasma equilibrium reconstruction, Tech, Phys, Lett. **49** 4 (2023) 372-375.
[14]. KURSKIEV G.S., et al. "Neutral beam injection for electron heating of Globus-M2 spherical tokamak's plasma" 30th IAEA Fusion Energy Conference (Chengdu, People's Republic of China, 2025)
[15]. KISELEV E.G., et al. "Gyrokinetic linear simulation of hot ion mode in Globus-M2 spherical tokamak" 30th IAEA Fusion Energy Conference (Chengdu, People's Republic of China, 2025).
[16]. MCNAMARA, S. A., ASUNTA, O., BLAND, J., et. al. Achievement of ion temperatures in excess of 100 million degrees Kelvin in the compact high-field spherical tokamak ST40, Nucl. Fusion. **63** 5 (2023) 054002.
[17]. KAYE, S. M., SERTOLI, M., BUXTON, P., et. al. Isotope dependence of transport in ST40 hot ion mode plasmas, Plasma Phys. Control. Fusion. **65** 9 (2023) 095012.
[18]. MUKHIN E.E., et al. "High-field-side high-density region in Globus-M2 divertor" 30th IAEA Fusion Energy Conference (Chengdu, People's Republic of China, 2025).
[19]. BONNIN, X., DEKEYSER, W., PITTS, R., et al. Presentation of the new SOLPS-ITER code package for tokamak plasma edge modelling, Plasma Fusion Res. **11** (2016) 1403102.
[20]. VEKSHINA, E., ROZHANSKY, V., KAVEEVA, E., et al. Modelling of Globus-M connected double null discharge, Plasma Phys. Control. Fusion. **61** 12 (2019) 125009.
[21]. DOLGOVA, K., VEKSHINA, E., ROZHANSKY, V. Modeling of high-field-side high-density regime in the Globus-M2 tokamak, Plasma Physics and Controlled Fusion. **66** 3 (2024) 035001.
[22]. ERMAKOV, N. V., ZHILTSOV, N. S., KURSKIEV, G. S., et al. Divertor Thomson Scattering on Globus-M2, Plasma Physics Reports. **49** 12 (2023) 1480-1489.
[23]. EICH, T., SIEGLIN, B., SCARABOSIO, A. et al. Inter-ELM Power Decay Length for JET and ASDEX Upgrade: Measurement and Comparison with Heuristic Drift-Based Model, Phys. rev. lett. **107** 21 (2001) 215001.
[24]. EICH, T., LEONARD, A. W., PITTS, R. A., et al. Scaling of the tokamak near the scrape-off layer H-mode power width and implications for ITER, Nucl. Fusion. **53** 9 (2013) 093031.
[25]. PONOMARENKO A. et al. "The study of alfvén eigenmodes on the spherical tokamak globus-m2 using doppler backscattering" 30th IAEA Fusion Energy Conference (Chengdu, People's Republic of China, 2025)

[26]. BALACHENKOV, I. M., PETROV, Y. V., GUSEV, V. K., et al. Effect of plasma toroidal rotation on toroidal Alfvén eigenmode spectrum in Globus-M2 spherical tokamak, Plasma Phys. Reports. **50** 7 (2024) 765.

[27]. SKREKEL O.M., et al. "Study of fast ion transport and losses during alfvén type mhd instabilities at Globus-M2" 30th IAEA Fusion Energy Conference (Chengdu, People's Republic of China, 2025).

[28]. BAKHAREV N.N., BALACHENKOV I.M., VARFOLOMEEV V.I et al. Heat Load onto the Globus-M2 Tokamak Wall due to Fast Ion Loss during Development of Toroidal Alfvén Eigenmodes, Plasma Phys. Rep. **49** 12 (2023) 1317-1326.

[29]. YASHIN A.Y. et al. "First Observations of the Transition to the H-Mode on the Globus-M2 Tokamak using Doppler Backscattering" 29th IAEA Fusion Energy Conference (London, United Kingdom, 2023)

[30]. PONOMARENKO, A., GUSEV, V., KISELEV, E., et al. The investigation of edge-localized modes on the Globus-M2 tokamak using Doppler backscattering, Nuclear Fusion. **64** 2 (2023) 022001.

[31]. TOKAREV, A. Y., YASHIN, A. Y., PONOMARENKO, A. M., et al. Application of multi-frequency doppler backscattering for studying edge localized modes at the Globus-M2 tokamak, Plasma Phys. Rep. **50** 5 (2024) 541-551.

[32]. YASHIN, A. Y., BAKHAREV N.N., BUTS M. et al. Experimental study of small ELMs on the spherical Globus-M2 tokamak, Physics of Plasmas. To be published.

[33]. SOLOKHA, V. V., et al. "Numerical analysis of peeling-ballooning stability at various triangularities in globus-m2" 30th IAEA Fusion Energy Conference (Chengdu, People's Republic of China, 2025)

[34]. SOLOKHA, V. V., BALACHENKOV, I. M., GUSEV, V. K., et al., Observation of peeling-ballooning destabilization at low pressures in weakly shaped Globus-M2 discharges, Phys. Plasmas. **32** 5 (2025) 052505.

[35]. DUDSON B., et al., BOUT++: A framework for parallel plasma fluid simulations, Comput. Phys. Commun. 180, 1467–1480 (2009).

[36]. YASHIN, A. Y., et al "First results of eho-like fluctuations studies at the spherical tokamak Globus-M2" 30th IAEA Fusion Energy Conference (Chengdu, People's Republic of China, 2025)

[37]. KULYGIN, M. S., BALACHENKOV, I. M., BAKHAREV, N. N., et al. First observations of ion cyclotron emisison in the spherical tokamak Globus-M2, Tech. Phys. Lett. **50** 18 (2024) 71-75.

[38]. BALACHENKOV, I. M., BAKHAREV, N. N., GUSEV, V. K., et al. Chirping instabilities produced by a runaway electron beam at a spherical tokamak, Plasma Science and Technology. **25** 7 (2023) 075102.